**Migration Letters**

Volume: 21, No: S10 (2024), pp. 380-394

ISSN: 1741-8984 (Print) ISSN: 1741-8992 (Online)

www.migrationletters.com

# Study On The Use Of Inverse Fluidized Bed Technology To Treat Wastewater By Eliminating Dye Pollutants From The Al-Kut Textile And Knitting Factory

Sadiq Mussadaq M Baqer , Hatem A Gzar , Mahdi Nuhair Rahi , Qasim M Jani

## Abstract

***Aim of the Study****: The study aims to investigate the effectiveness of Inverse Fluidized Bed Technology (IFBT) for the sustainable removal of terasil blue dye from Al-Kut Textile and Knitting Factory wastewater. Additionally, the research focuses on evaluating the role of adsorbent styles, specifically modified rice husks, in the absorption of terasil blue dye from wastewater.*

***Mechanism and Methodology****: In this work, to remove the terasil blue dye from wastewater coming from Kut Textile and Knitting factory used IFBT to safeguard biofilm and facilitate re-fluidization during power outages in wastewater treatment. An adsorption method has applied to analyze and removal of terasil blue dye from the water treatment in Kut Textile and Knitting Factory. The terasil blue dye adsorption was performed using rice husk as the adsorbent in batch mode by varying parameters such as pH, particle size of rice husks and it's dose, contact time and terasil blue dye concentration. Further, kinetics of the adsorption of the dye on rice husks was investigated.*

***Results****: The terasil blue dye removal usi[1]ng rice husks adsorbent showed that various parameters including the pH, particle size of rice husks and it's dose, contact time and terasil blue dye concentration. The experimental results indicated that the maximum removal efficiency obtained to be 97.15%, at a fixed 200 RPM agitation speed, pH of 7, with 200 minutes contact time, rice husks' particle size of 1.18 to 2.35 mm and an adsorbent mass of 4 g. The particle size rice husks adsorbent is identified as it positive influences on removal efficiency. Rate constants at varied concentrations are provided to offer insights into the kinetics of the adsorption process. The adsorptive removal efficiencies were obtained at temperature 25±1 °C and initial dye concentration 20 mg/L. Langmuir, Freundlich and isotherm models revealed that Freundlich and isotherm models were best model for terasil blue adsorption. Equilibrium and adsorption dynamics are visually represented in figures, providing a comprehensive overview of the outcomes.*

***Conclusion****: The comprehensive data analysis presented throughout the study underscores the real-world applicability of modified rice husks in the context of improving the efficiency of wastewater treatment processes. The study recommends the application of IFBT for treating Al-Kut Textile and Knitting Factory effluent, specifically targeting color pollutants. This work emphasizes the significance of modified rice husks, and eco-friendly, cost-effective alternatives in wastewater treatment.*

**Keywords:** Hydrodynamics, Liquid-Solid Inverse Fluidization, Carbon, Rice husks.

## 1. INTRODUCTION

Civil Engineering Department College of Engineering, Waist University Waist, Iraq.

Hydrodynamics and liquid-solid inverse fluidization are explored in various applications [1]. It also includes smooth circular or columnar reverse fluidized beds with sloped or tapering sections in inverted reactors. A unique velocity profile arriving from the top and departing from the bottom gives these reactors high power consumption. On the other hand, power savings, and easier fluidization during power outages are also part of this function [2]. Tapered inverted fluidized bed reactors are used in aerogel-based oil-water separation, biofilm growth, and COD, BOD, and TOC reduction.

Despite its expensive cost, activated carbon powder can remove industrial colours due to its large surface area and high absorbency [3]. Absorbent compounds like "trail blue dye" and "rice husks" affect feeding, process column, primary attention, bed depth, and flow rate, exposing breakthrough dependencies. Conocarpus uses chemically treated or untreated adsorbents [4]. Experimental bed design affects minimum "fluidization" pressure and velocity declines [1-6]. “Three-phase fluidized-bed bioreactors (TPIFB)” performance depends on retention duration, bio-carriers, reactor aspect ratio, surrounding skin flow rate, surface liquid velocity, bed expansion, and mass transfer coefficient. Fluid velocity and particle properties affect "biofilm substrate porosity," with rising gas velocity increasing mass transfer (kLa) in an inverted three-phase fluidized bed [7].

For Residence Time Distribution (RTD) studies using solids as tracers, CFD simulations are used and confirmed experimentally in a conventional fluidized bed [3,4]. Fluidized bed reactors differ from fixed-bed reactors in how they fluidize solids. A fluidized bed reactor must have a solid-to-liquid density ratio greater than one, unlike a fixed-bed reactor. Fluid flows continuously with gas in a fixed-bed reactor [4]. The hydrodynamic operating regimes of two- and three-phase Inverse Fluid Bed Reactors (IFBR) make them more effective than up-flow fluidized bed reactors for wastewater bioremediation in Iraq [5]. Post-biological or chemical oxidation, wastewater treatment plants adsorb terasil blue dye to remove dissolved contaminants. Hydrodynamic studies of the inverse fluidized bed reactor predict bed expansion and phase holdups using low-density particles of various sizes and densities [7,8].

The Inverse Fluidized Bed Reactor (IFBR) prevents biofilm peel-off and facilitates re-fluidization during power outages with high mass transfer rates and minimal particle attrition. Bioprocessing aerobic and anaerobic wastewater now requires IFBR [8]. Despite minimal study on IFBR hydrodynamics with different particle densities and sizes, cork and polyethene nanoparticle studies examine minimum fluidization velocity and friction factor connections. The Response Surface Method (RSM) evaluates many variables and their interactions with fewer experimental trials, helping analyze complicated interactions and determine optimal operational settings [9,10]. Introduce gas into the sparger to optimize solid "fluidization" throughout the three phases of an "inverse fluidized" bed, with sparger size affecting efficiency [10]. Time, surface gas velocity, aspect ratio, and settled bed volume to working volume (Vb/Vr) affect wastewater treatment performance [11]. Weight loss per unit measurement peaks with cumulative liquid flow rate and decreases as the bed extends to regulate the hydrodynamics of a three-phase "inverse fluidized bed." Natural loading, maintenance time, and waste concentration affect reverse fluidized-bed bioreactor wastewater treatment. Despite probable bed compaction due to native agitation by air pockets near the least "liquid fluidization velocity" [12], three-phase structures have a lower minimum "fluidization voidage" than two-phase structures. The minimum "fluidization velocity" falls as the wetting agent is introduced to the liquid downflow in a three-phase inverse fluidized bed. Gas bubbles often enter an inverted phase "fluidized" bed and flow downward with the liquid, affecting hydrodynamic measurements without changing the bed's major hydrodynamic state [13,14].

Biological selenium removal technologies are promising due to their low cost, high treatment efficiency, adaptability for low effluent concentration, and sustainability. Several bacteria that use selenium as a terminal electron acceptor use dissimilatory reduction of selenium oxyanions for anaerobic respiration. Converting soluble selenate and selenite to

elemental selenium nanoparticles decreases selenium's toxicity and bioavailability, enabling bioremediation and the creation of selenium nanospheres for diverse uses [15]. Selenium nanoparticles are used in semiconductors with antimicrobial coatings, light emitting diodes, solar cells, biological imaging, and heavy metal adsorption. Selenium nanoparticle synthesis and wastewater treatment by microbes are industrially attractive and economically viable [16].

This study uses inverse fluidized bed technology (IFBT) to remove terasil blue dye from polluted industrial waste water from the Al-Kut Textile and Knitting factory. The terasil blue dye adsorption was performed using rice husk as the adsorbent in batch mode by varying parameters such as pH, particle size of rice husks and it's dose, contact time and terasil blue dye concentration. Further, kinetics of the adsorption of the dye on rice husks was investigated. Additionally, it also aims to describe and determine appropriate hydrodynamic parameters in an inverse fluidized bed process.

## 2. EXPERIMENTAL

### 2.1. Preparation of Rice husk

Rice husks, obtained locally in Iraq, were cleaned thoroughly and treated with a 0.1 N NaOH solution for 24 hours to prepare the adsorbent. After rinsing with distilled water, the modified rice husks were dried at 60°C for 24 hours using a Binder drying oven (ED series, Germany) [17]. After drying, the modified rice husks will be ground and sieved to achieve particles ranging from 1.18 to 2 mm, enhancing surface area and adsorption capacity. Activation for increased adsorption efficiency will be conducted by subjecting the modified rice husks to a two-hour treatment in a 300°C electric muffle furnace [18]. This process results in an adsorbent with a large surface area and an increased adsorption capacity, making it effective in removing impurities from wastewater [19].

### 2.2. Preparation of TB

To prepare the terasil blue solution, 20 mg of the dye was dissolved in 1000 ml of tap water. The dye components (Table 1) were analyzed with an EDS device (Type x-act, USA). From the stock solution, concentrations (20 mg/L) of terasil blue (TB) dye was prepared by diluting with water [20]. These concentrations of TB solution were used to construct a calibration curve, relating TB concentrations to absorbance. In our experiments, a concentration of 10 mg/L of TB dye was used.

### 2.3. Inverse fluidized bed experiments

Figure 1 shows a schematic diagram of the inverse fluidized bed reactor. It consists of (1) Feed Tank, (2) Liquid Pump, (3) Control Valve, (4)) recycle flow pipe, (5) Liquid Rotameter, (6) Pipe Fitting Plug, (7) Air Vent Valve, (8) Inverse Fluidization Column, (9) Manometer (10) Drain Tank. The inverse fluidized system has equipment with: (i) A circular steel tank with a capacity of 50 liters is used to feed wastewater into the column, (ii) A polyethylene container with a capacity of 50 liters is used to collect the effluent solution, (iii) The Perspex column has a diameter of 50 mm externally, 43 mm internally, and a height of 1000 mm. Various fittings such as PVC flanges, hoses of different sizes, and pipes are used to connect the column, (iv) Plastic distributors are placed at the top and bottom of the column, (v) A Rotameter is used to calculate the rate of flow of the influent, that ranges between 0-0.2 L/min of water, (vi) A 0.5 hp centrifugal pump transfers contaminated water from a feed tank to a column, maintaining consistent intake by recycling a portion back to the feed container.

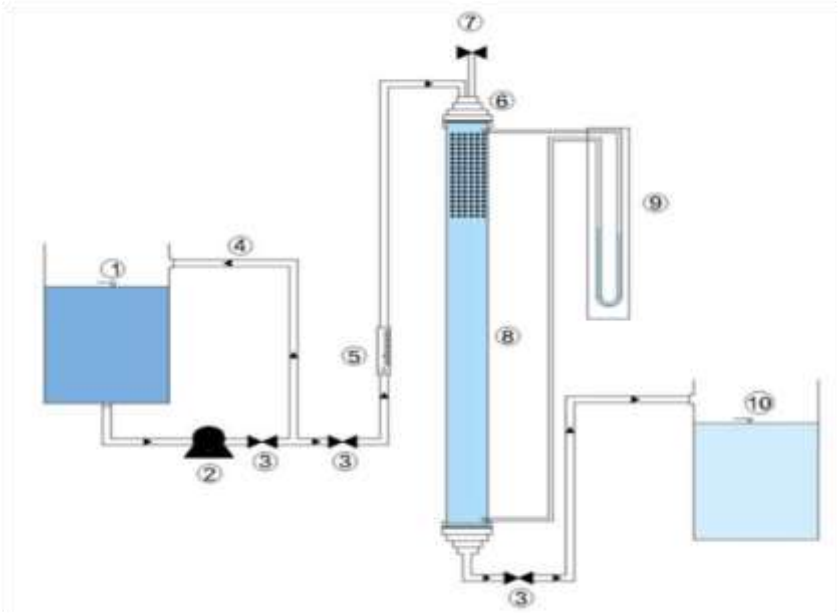


**Figure 1:** Schematic Representation of Inverse Fluidized Bed Reactor

The experiment can be performed by using a setup (Figure 1), with a rising fluid from a reservoir driven into the reactor's surface by centrifugal force. Prior to entering the bed, the fluid was aerated through a sparger, with air blown in via a distributor. The fluidized bed section was 15 cm in diameter and 6 m in height, followed by an uncoupling cap. The dimensions influenced fluid and air flow, as well as bed particle compression resistance. Detached biomass was collected from the effluent. Liquid flow was measured with a rotameter (4), airflow with a rotameter (5). A control system (3) with a pH meter and micropumps maintained pH, and temperature was controlled using a coil, electric heater, and contact thermometer.

### 2.4. Batch experiments

Using a rice husk adsorbent, the experiment on the adsorption of terasil blue dye was carried out in batch mode by varying the adsorption parameters, including pH, temperature, dose level, metal ion concentration, and period of contact. The optimum adsorption parameters were determined by adjusting the pH from 3.0 to 9.0 at 25°C, using starting concentration of 20 mg/L of dye in 100 mL solution. Using a higher concentration of dye helps to reduce the variability in the experimental results and ensure that the adsorption is efficient and that the experimental work is reproducible. The contact time of 200 minutes was kept with a rice husk quantity of 0.5-5 g/L. The experiment system was continuously stirred for 200 minutes to ensure achieving the equilibrium. The effect of contact time was also inspected by changing the time breaks of the rice husk from 20 to 200 minutes, and the extent of adsorption onto the absorbent was evaluated at several time periods using Eq. (1).

$$q_e = \frac{(C_o - C_t)V}{m} \qquad [1]$$

Here, $C_0$ represents the starting concentration (mg/L) of the wastewater containing dye, $C_t$ represents the dye concentration at time t (mg/L), V represents the volume (L) of the wastewater, and m represents the mass (g) of the rice husk powder utilized as the absorbent.

A sample was collected and centrifuged at each time point, and the remaining concentration of adsorbed dye in the fluid stage was acquired after 5 minutes of centrifuging.

### 2.5. Instruments used for analysis

To evaluate the concentration of terasil blue dye a UV-Vis spectrophotometer (Shimadzu UV-1800) was performed by measuring the absorbance of the experimental dye solution were measured across a range of wavelengths. The initial and ending concentrations of blue dye present in the sample water before and after the adsorption method were measured using an Atomic Absorption Spectrometer (AAS) – AA7000 made by Shimadzu, Japan.

### 2.6. Kinetic studies

The equilibrium study varied dye concentrations (25 to 150 mg/L) with a 2 g/L dose of rice husk powder. The lower concentration ensured efficient adsorption, while the higher one explored concentration effects. The actual powder dose may vary based on its source and storage. At pH 5.0, 90 mL solutions were shaken at 150 rpm for an hour at 25°C. After purification, the adsorbed dye ($q_e$) was determined under equilibrium conditions using Eq. (2).

$$q_e = \frac{(C_o - C_e)V}{m}\ mg/g \qquad [2]$$

### 2.7. Adsorption isotherm study

Equilibrium adsorption isotherms for untreated and activated rice husk were determined at 150 rpm and room temperature using different concentrations of terasil blue dye. Ten grams per liter of adsorbent (based on the dry weight of rice husk) were placed in 250-mL Erlenmeyer flasks, each containing varying initial terasil blue dye concentrations (5, 10, 15, 20, and 25 mg/l). The experiments aimed to estimate maximum adsorption capacity, assess the impact of the activation process on adsorption, and understand adsorption behavior. After shaking for 2 hours, a sample was withdrawn, centrifuged at 4000 rpm for 5 minutes, and the supernatant analyzed for terasil blue dye content. All experiments were conducted in duplicate with a relative deviation of less than 5%. The adsorption behavior was assessed by calculating the percentage removal efficiency of terasil blue dye [21] using Eq. (3):

$$\text{Removal efficiency} = \frac{(C_o - C_e)}{C_o} \times 100 \qquad [3]$$

where $C_0$ is the initial concentration of terasil blue dye, $C_e$ is the solution concentration after adsorption at any time.

The adsorption kinetics was assessed by studying the uptake of terasil blue dye from an aqueous solution at various time intervals. The adsorbed amount ($q_e$) of terasil blue dye on rice husk (mg/L) was calculated using the mass balance Eq. (4):

$$q_e = \frac{(C_o - C_e)V}{W}\ mg/g \qquad [4]$$

Where: $C_0$ = initial concentration, Ce = equilibrium concentrations (mg/L), V = volume, W = weight.

### 2.8. Equilibrium isotherms

Experiments were conducted to investigate equilibrium isotherms for optimizing the design of the terasil blue dye removal system from wastewater. These investigations were based on data obtained from the adsorbent dose study. The Eq. (5) was utilized to calculate the quantity of dye adsorbed at equilibrium, $q_e$. It was ensured that the obtained average values

fell within an error range of ±5%:

$$q_e = V_L \frac{(C_o - C_{e)}}{W_o} \qquad [5]$$

Where, $q_e$ represents the equilibrium uptake in milligrams per gram (mg/g), $V_L$ is the solution volume in liters (L), $C_0$ is the starting concentration in milligrams per liter (mg/L), $C_e$ is the equilibrium concentration in mg/L, and $W_0$ is the mass of adsorbent in grams (g).

The calculation of adsorption efficiency (η) was performed utilizing the subsequent Eq (6):

$$\eta = \frac{(C_0 - C_e)}{C_o} \text{x } 100 \qquad [6]$$

## 3. RESULTS

The ideal pH range (3-9) for the adsorption of terasil blue dye onto modified rice husk particles with a particle size of 1.18-2 mm is detailed in Table 1. Controlled parameters include a consistent adsorbent dose of 2 grams per 100 milliliters, a 150-minute contact period, a regulated temperature of 25°C, an initial dye concentration of 20 mg/L, and an agitation speed of 200 rpm. Dye adsorption capacity rose with increasing pH, following a trend from 14.04 mg/L at pH 3 to 17.92 mg/L at pH 7, and there afterwards no noticeable enahncement. Simultaneously, removal efficiency shows an increasing trend from 70.21% to 89.58%, at the pH 7 and then there is no recognigable change. The adsorption process is at its most efficient at pH 7, suggesting that neutral pH conditions are optimal for elimination. Insights into the dye's interactions with the modified rice husk particles as a function of pH are provided, which is useful for enhancing the adsorption process.

**Table 1:** Optimum pH for the adsorption of terasil blue dye onto modified rice husk particles

| **pH** | **$C_e$ (mg/L)** | **Amount Absorbed (mg/L)** | **Removal Efficiency (%)** |
|---|---|---|---|
| 3 | 5.96 | 14.04 | 70.21 |
| 4 | 4.64 | 15.36 | 76.78 |
| 5 | 4.02 | 15.98 | 79.92 |
| 6 | 3.77 | 16.23 | 81.46 |
| **7** | **2.08** | **17.92** | **89.58** |
| 8 | 2.28 | 17.72 | 88.61 |
| 9 | 2.25 | 17.75 | 88.74 |

Figure 2 displays the correlation between particle size (from 1.18 to 2.35 mm, 3.35 to 4.25 mm, and 4.25 to 6 mm) and terasil blue adsorption removal effectiveness. Removal efficiencies of 94.1%, 92.3%, and 90.2% are displayed on the Figure 2 (Particle size Vs Removal efficiency), indicating a general downward trend. According to the provided context, there appears to be an effective first adsorption phase with a low Ce/qe that saturates with time, revealing the adsorbent's finite capacity (Ce). Adsorption of terasil blue dye on the designated adsorbent is shown to be effective and to exhibit dynamic saturation based on particle size.

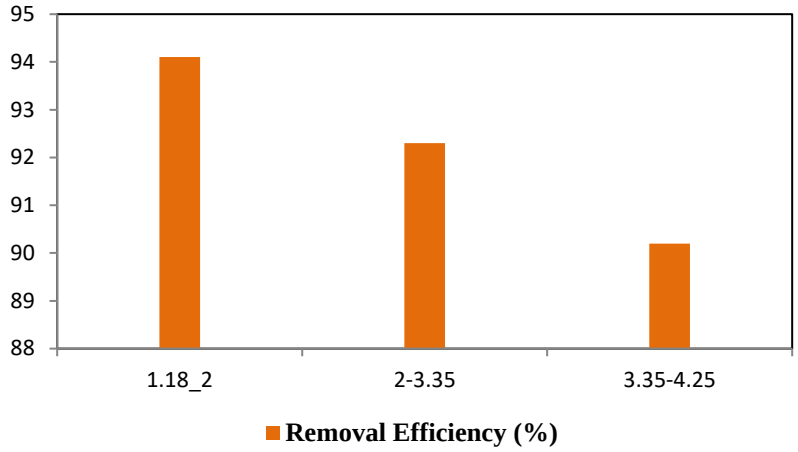


**Figure 2:** Optimum particle size for the adsorption of terasil blue dye onto modified rice husk particles (1.18-2 mm particle size).

Table 2 shows how adsorbent mass and agitation speed influence terasil blue dye adsorption most effectively. There is a positive relationship between adsorbent mass and adsorption performance, as the amount absorbed increases from 11.34 mg/L to 19.43 mg/L and the removal efficiency increases from 56.72% to 97.15% as the adsorbent mass are increased from 0.5 g to 4 g. Then, the removal efficiency rose somewhat from 86.62% to 92.23% when agitation speed rises from 125 to 200 RPM. Further increase in agitation speed causes to decrement of removal efficiency, so, a RPM of 200 was optimized. These results shed light on how to best adjust adsorbent mass and agitation speed to maximize dye removal.

**Table 2:** Optimum effect of adsorbent mass

| **Adsorbent Mass (g)** | **(mg/L)** | **Amount Absorbed** | **Removal Efficiency** |
|---|---|---|---|
| 0.5 | 11.34 | 8.66 | 56.72 |
| 1 | 12.55 | 7.45 | 62.74 |
| 2 | 14.87 | 5.13 | 74.36 |
| 3 | 18.74 | 1.26 | 93.7 |
| **4** | **19.43** | 0.57 | **97.15** |
| **Agitation speed** | **(mg/L)** | **Amount Absorbed** | **Removal Efficiency** |
| 125 | 2.68 | 17.32 | 86.62 |
| 150 | 2.02 | 17.98 | 89.91 |
| **200** | **1.55** | **18.45** | **92.23** |
| 250 | 1.63 | 18.37 | 91.92 |

Table 3 shows how the contact time influences the adsorption of terasil blue dye, displaying a range of absorbed amounts and removal efficiencies. The elimination efficiency increases from 40.6% to 87.59%, and the amount absorbed drops from 11.88 mg/L to 2.48 mg/L, as contact duration increases from 120 minutes to 200 minutes and thereafter a slight decrease

was observed. This implies that there's an optimal contact time at 200 minutes, where maximum removal effectiveness of 87.59% is attained. After that point, every more time spent in close proximity has a declining return. The information is useful for calculating the optimum time required for the adsorption process, which in turn optimizes the efficacy of the removal process.

**Table 3:** Optimum contact time

| **Time (min)** | **(mg/L)** | **Amount Absorbed (mg/L)** | **Removal Efficiency (%)** |
|---|---|---|---|
| 120 | 11.88 | 8.12 | 40.6 |
| 150 | 7.74 | 12.26 | 61.32 |
| 180 | 4.51 | 15.49 | 77.47 |
| **200** | **2.48** | **17.52** | **87.59** |
| 210 | 3.03 | 16.97 | 84.87 |

The rate constant K ($min^{-1}$) quantifies the rate at which the adsorption process takes place. A greater rate constant corresponds to an increased rate of adsorption. The K values for the adsorption of terasil blue onto activated and untreated rice husks at different concentrations are shown in Table 4. The rate constant for activated rice husk varies between 0.013 and 0.079 $min^{-1}$ as the dye concentration is increased from 5.0 to 25 mg/L with 5-10 g/L of adsorbent. A strong relationship between adsorbent concentration and rate constant is indicated by the correlation coefficient (r) values. Similar concentration-dependent rate constant, with a peak of 0.089 $min^{-1}$, was seen in unprocessed rice husks. High values of r indicate a significant relationship. These results are helpful for deciphering the kinetics of terasil blue adsorption, which depends on the type and concentration of the adsorbent used.

**Table 4:** Rate constants for the adsorption of terasil blue on untreated and citric acid treated rice husk

| **Adsorbent type** | **Concentration of Adsorbent (g/L)** | **Concentration of Dye (mg/L)** | **Rate constant K ($min^{-1}$)** | **r value** |
|---|---|---|---|---|
| Activated Rice husk | 5.0 | 5<br>10<br>15<br>20<br>25 | 0.013<br>0.016<br>0.018<br>0.032<br>0.011 | 0.90<br>0.98<br>0.91<br>0.95<br>0.97 |
| | 10 | 5<br>10<br>15<br>20<br>25 | 0.079<br>0.075<br>0.040<br>0.022<br>0.027 | 0.97<br>0.96<br>0.98<br>0.92<br>0.96 |
| Untreated Rice husk | 5.0 | 5<br>10<br>15<br>20<br>25 | 0.040<br>0.034<br>0.036<br>0.036<br>0.033 | 0.97<br>0.98<br>0.95<br>0.99<br>0.98 |

| | | | | |
|---|---|---|---|---|
| | 10 | 5 | 0.053 | 0.95 |
| | | 10 | 0.056 | 0.99 |
| | | 15 | 0.089 | 0.98 |
| | | 20 | 0.047 | 0.92 |
| | | 25 | 0.051 | 0.94 |

Figure 3 (Equilibrium isotherms for adsorption of Terasil blue dye) shows mathematical models, Langmuir, Freundlich, and Temkin models with the correlation between terasil blue adsorption's initial concentration (x), adsorption capacity (y), equilibrium concentration ($C_e$), and adsorption amount ($q_e$). The plot demonstrates a fast adsorption phase early on, with $C_e/q_e$ ratios that are low. The plot, however, also shows saturation developing with time, indicating that the adsorbent has a finite capacity ($C_e$). $C_e$'s natural logarithm is also shown, emphasizing how adsorption efficiency drops down toward equilibrium. Understanding the equilibrium between the initial efficiency and the adsorbent's capacity is highlighted by this visual representation of the kinetics of terasil blue adsorption.

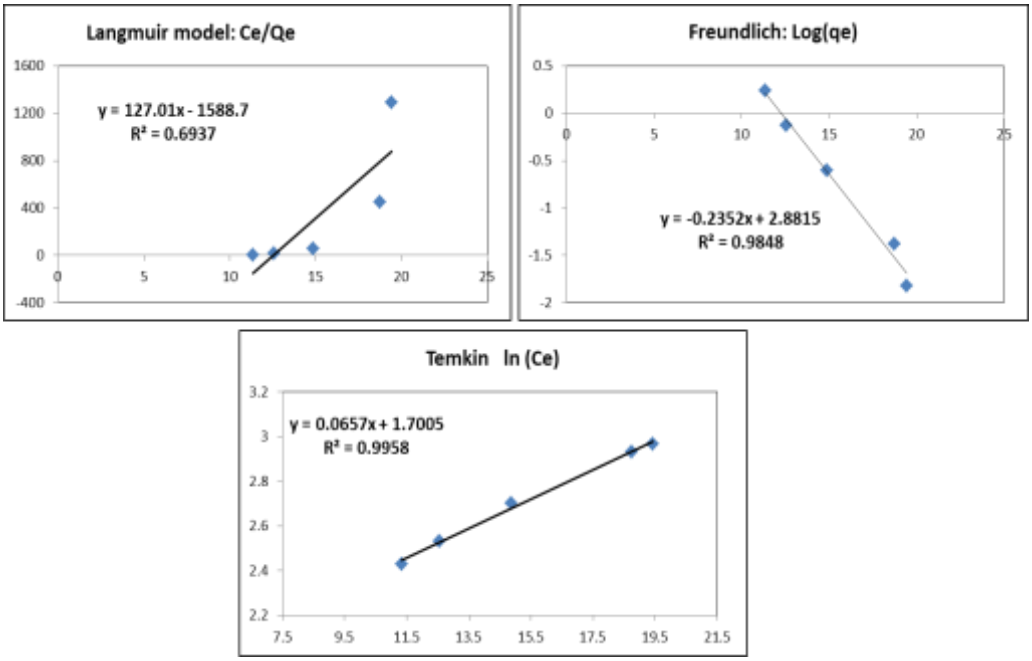


**Figure 3:** The plot demonstrates efficient initial adsorption (low $C_e/qe$) which saturates over time, indicating the adsorbent's limited capacity ($C_e$)

Table 5 shows data analysis reveals significant variations in adsorption characteristics, emphasizing the influence of initial concentration ($C_e$), equilibrium adsorption capacity ($q_e$), and logarithm of $C_e$(ln ($C_e$)) on the adsorption process. Langmuir, Freundlich and isotherm models revealed that Freundlich and isotherm models were best model for terasil blue adsorption.

**Table 5:** The data analysis reveals significant variations in adsorption characteristics

| **Isotherm Model** | **Parameter** | **Value of Tarasil blue** |
|---|---|---|
| Langmuir Isotherm | $q_{max}$ (mg/g) | 0.0078 |
| | $K_L$ (L/mg) | 0.0801 |
| | $R_L$ | 0.382 |
| | $R^2$ | 0.6937 |

| | | |
|---|---|---|
| Freundlich Isotherm | 1/n | 4.25 |
| | $K_f$ (mg/g . $(L/mg)^{\frac{1}{n}}$) | 2.51 |
| | $R^2$ | 0.9848 |
| Temkin Isotherm | $B_T$ (J/mol) | 0.0657 |
| | $K_T$(L/mg) | 1.454 |
| | $R^2$ | 0.9958 |

Figure 4 displays the logarithmic variation in ($q_e$ - $q_t$) over time (t), illustrating the dynamics of terasil blue adsorption. Log($q_e$ - $q_t$) values decrease over time, indicating a slowing pace of change. This indicates that the adsorption process is progressing toward equilibrium as the difference between $q_e$ and $q_t$ decreases. As the system approaches saturation, the rate of adsorption decreases, as indicated by the negative trend in log($q_e$ - $q_t$). The strong $R^2$ value of 0.9356 indicates how well the trend is represented, highlighting the time-varying dynamics of adsorption.

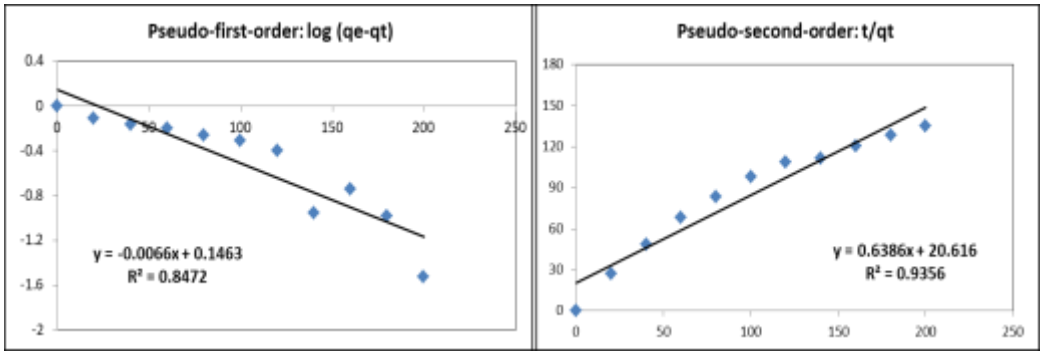


**Figure 4:** The rate of change in −log($q_e$ - $q_t$) decreases with time, indicating a gradual reduction in the difference between $q_e$ and $q_t$.

In Figure 5, the plotted experimental data demonstrates a nonlinear relationship between the square root of time ($t_{1/2}$) and the negative of adsorbed quantity (-$q_t$). This nonlinearity could indicate that the removal effectiveness in the adsorption process is complex and even time dependent. The size of -$q_t$ grows with increasing $t_{1/2}$, highlighting a correlation between $t_{1/2}$ and the efficacy of the adsorption mechanism. The complex nature of the shown connection emphasizes the importance of a fine-grained comprehension of the temporal dynamics impacting the removal efficiency in this particular adsorption process.

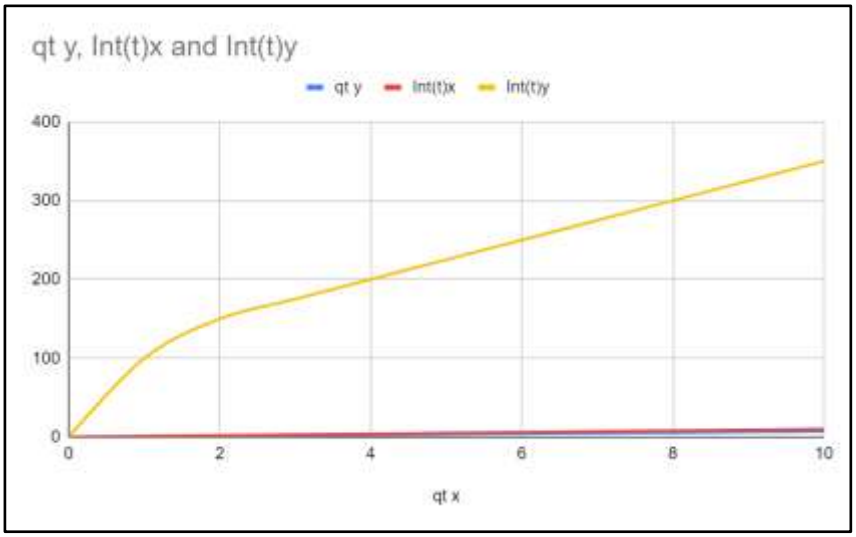

**Figure 5:** The experimental data demonstrates a nonlinear relationship between $t_{1/2}$ and $-q_t$, indicating a complex dependency between time and the removal efficiency of the process.

Table 6 shows the pressure decrease (in Pascals) for two distinct masses (0.04 kg and 0.06 kg) and two different bed heights (10 cm and 20 cm) for four different surface fluid velocities (U). Pressure drops tend to grow when the speed of fluids near the surface rises. Furthermore, at a given velocity, bed height and mass have an appreciable effect on pressure decrease. Higher bed heights and masses lead to increased pressure decreases. This information is essential for engineering applications, especially in fluidized bed systems, since it sheds light on the connection between fluid dynamics, bed properties, and pressure decreases.

**Table 6:** Pressure drops vs. superficial fluid velocity

| **?Velocity U (m/s)** | **Mass of 0.04 kg** | **Mass of 0.06 kg** |
|---|---|---|
| **∆P (Pa)** | | |
| 0.009 | 78 | 108 |
| 0.016 | 98 | 147 |
| 0.027 | 118 | 177 |
| 0.031 | 147 | 275 |
| 0.043 | 206 | 333 |
| 0.056 | 265 | 431 |
| 0.069 | 324 | 461 |
| 0.071 | 333 | 490 |
| 0.075 | 343 | 510 |
| 0.081 | 333 | 520 |
| 0.086 | 353 | 510 |
| Superficial fluid Velocity U (m/s) | Bed Height 10 (cm) Mass of0.04 (Kg) | Bed Height 20 (cm) Mass of 0.06 (Kg) |
| 0 | 10 | 20 |
| 0.009 | 10 | 20 |
| 0.016 | 11.4 | 21.3 |
| 0.027 | 13 | 22 |
| 0.031 | 14.2 | 22.5 |
| 0.043 | 14.8 | 23.2 |
| 0.056 | 15.3 | 24 |
| 0.069 | 16 | 25.7 |

| | | |
|---|---|---|
| 0.071 | 17.2 | 27 |
| 0.075 | 18 | 28.1 |
| 0.081 | 19.1 | 29.4 |
| 0.086 | 20 | 30.7 |

## 4. DISCUSSION

The study found that the adsorption capacity of rice husk for terasil blue dye rises with higher dye concentration and sorbent dosage. The maximum adsorption occurs with activated rice husk at a sorbent dosage of 10.0 g/l and a terasil blue dye concentration of 25.0 mg/l. The adsorption kinetics aligns with a pseudo-second-order model, suggesting that the process is governed by the diffusion rate of terasil blue dye molecules into the rice husk pores [22]. The activated rice husk was found to be more effective than the untreated rice husk, due to its increased surface area and porosity. The pseudo-second-order model can be used to predict the adsorption kinetics of terasil blue dye on rice husk [23]. The isotherm allows for the approximation of the acceptance at equilibrium ($q_e$), which can impact the system arrangement and utilized to compare the potential of different adsorbent forms. Additionally, the isotherm is important for evaluating the likelihood of gaining the desired level of clarity of the adsorbent, especially in cases where multiple contaminants are existent and few toxins are only partly absorbed. Researchers have noted that the isotherm is an essential tool for studying the desorption process and understanding the association between adsorbents and adsorbates.

The bed heights in Figure 6 are displayed at three separate periods in time throughout the experimental hydrodynamics research. The bed in the first picture (a) is 20 centimetres off the ground. Before any liquid is introduced to the column, the bed will be at this height. The second picture (b) shows a 33 cm higher bed than the first. After the liquid has been added and the column has been running for some time, the bed height will be at this point. The bed's height increased to 37 cm in figure 3c. This is the bed height after the column has been worked for a longer time [24, 25]. The bed rises because the particles in the bed expand as they come into touch with the liquid. The particles absorb the liquid and grow in size. The particles disperse and the bed rises as a result of the swelling. In Langmuir and Freundlich models, adsorption isotherms explain solute equilibrium between liquid and solid phases. Freundlich model quantifies multilayer sorption, while Langmuir quantifies monolayer sorption. Studies of copper, nickel, and chromium adsorption have used the Temkin model and various isotherms. PSO has superior correlation in various adsorption systems, hence the pseudo-first-order (PFO) and pseudo-second-order (PSO) kinetic models are commonly used [26]. Terasil blue dye adsorption onto rice husks can be modelled using several models. Some models assume that colour adsorption onto rice husks is reversible and linear, such as the Langmuir isotherm. As a function of solution dye concentration, the Langmuir isotherm predicts rice husk equilibrium uptake of terasil blue dye. In addition, the model can determine the maximal dye adsorption per rice husk mass. Several models can describe terasil blue dye absorption onto rice husks.


**Figure 6:** Bed Expansion in the Inverse Fluidization

Specific experimental conditions and required accuracy determine model selection [27]. Our investigation used Langmuir isotherm modelling. The model's equilibrium uptake of terasil blue dye was compared to experimental data to validate it. Validation demonstrated that the model was accurate and could predict. According to the modelling simulations, rice husks' equilibrium uptake of terasil blue dye increased with dye concentration. The model evaluated rice husks' maximal dye adsorption per mass. The adsorption rate started fast and slowed as equilibrium neared. The study affects wastewater terasil blue dye adsorption system design and operation. The modelling simulations can optimise the adsorption system to remove the most terasil blue dye from wastewater. The batch and inverse fluidization column experiments to remove terasil blue dye from wastewater using rice husk as an absorbent. The fluidization of solid particles is essential in adsorption systems. If solid particles are fluidized with liquid flowing downward, inverse fluidization is energy-efficient due to its lower energy requirements and increased turbulence. After hydrothermal carbonization, rice husk particles have enhanced density and external porosity for biofuel use. This extensive study emphasizes the efficacy of natural and waste materials as adsorbents for wastewater treatment. Researching inverse fluidization and rice husks as an adsorbent helps environmental remediation [28].

## 5. CONCLUSION

This study concluded that the use of inverse fluidized bed technology to treat wastewater from the Al-Kut Textile and Knitting factory the removal of terasil blue dye. The study used less expensive and naturally available rice husks as adsorbent for the adsorption of terasil blue dye pollutant from wastewater effluents from the factory. In this work optimized the experimental design, statistical analysis, and adsorption outcomes. The optimal pH, particle size, adsorbent mass, agitation speed, and contact time for terasil blue dye removal with modified rice husks were determined. The data obtained indicate that the equilibrium isotherms for terasil blue adsorption onto rice husks as adsorbent are of the favorable for application for the removal of dyes from waste water. Using natural and waste materials like rice husks makes the suggested method eco-friendly and cost-effective. The developed technique could help to eliminate dye pollutants from industrial wastewater, enabling sustainable and effective wastewater treatment.

## 6. REFERENCES

1. Wang, L., Zhu, J., Nakhla, G. and Shao, Y., 2021. The hydrodynamics of liquid-solid and gas-liquid-solid inverse fluidized beds with bioparticles. Advanced Powder Technology, 32(1), pp.254-265.
2. Sakhile, K., Sarkar, J.P., Gupta, P., Shaik, F. and Lakkimsetty, N.R., 2023. Effect of Physical Properties of Solid Particles and Liquid Media on the Hydrodynamics of a Liquid–Solid Inverse Fluidized Bed. Arabian Journal for Science and Engineering, pp.1-16.
3. Sang, L., Nan, T., Jaberi, A. and Zhu, J., 2020. On the basic hydrodynamics of inverse liquid-solid circulating fluidized bed downer. Powder Technology, 365, pp.74-82.
4. Chen, S., Li, R., Ma, K., Shao, Y. and Zhu, J., 2022. Hydrodynamic characteristics of a pilot-scale gas-driven inverse liquid-solid fluidized bed with a central draft tube. Chemical Engineering and Processing-Process Intensification, 180, p.108999.
5. Nan, T. and Zhu, J., 2022. Hydrodynamics of inverse liquid-solid circulating fluidized bed. Chemical Engineering Science, 248, p.117187.
6. Song, Y., Sun, Z., Zhang, C., Zhu, J. and Lu, X., 2019. Numerical study on liquid-solid flow characteristics in inverse circulating fluidized beds. Advanced Powder Technology, 30(2), pp.317-329.
7. Deng, Y., Ma, K., Huang, J., Shao, Y. and Zhu, J., 2023. Hydrodynamic characteristics of a rectangular gas-driven inverse liquid-solid fluidized bed.Particuology, 78, pp.86-96.
8. Nan, T. and Zhu, J., 2022. Hydrodynamics of an inverse liquid–solid circulating conventional fluidized bed. AIChE Journal, 68(4), p.e17593.
9. Huang, J. and Zhu, J., 2021. Hydrodynamics of a gas-driven inverse liquid-solid fluidized bed. The Canadian Journal of Chemical Engineering, 99(7), pp.1535-1545.
10. Mallikarjuna, C. and Dash, R.R., 2020. A review on hydrodynamic parameters and biofilm characteristics of inverse fluidized bed bioreactors for treating industrial wastewater. Journal of Environmental Chemical Engineering, 8(5), p.104233.
11. Das, L., Anand, P., Anjum, A., Aarif, M., Maurya, N., & Rana, A. (2023, December). The Impact of Smart Homes on Energy Efficiency and Sustainability. In 2023 10th IEEE Uttar Pradesh Section International Conference on Electrical, Electronics and Computer Engineering (UPCON) (Vol. 10, pp. 215-220). IEEE.
12. Srithong, K., & Limrattanaphattarakun, W. (2024). Guidelines for Developing the Potential of Farmer Organizations for Sustainable Self-Reliance. วารสาร สันติ ศึกษา ปริทรรศน์ ม จร, 12(2), 425-439.
13. Abd Algani, Y. M., Caro, O. J. M., Bravo, L. M. R., Kaur, C., Al Ansari, M. S., & Bala, B. K. (2023). Leaf disease identification and classification using optimized deep learning. Measurement: Sensors, 25, 100643.
14. Mishra, M. K., Selvaraj, K., Santosh, K., Aarif, M., Mary, S. S. C., & Bala, B. K. (2024, March). The Impact of 5G Technology on Agile Project Management: A Cross-Industry Analysis. In 2024 5th International Conference on Intelligent Communication Technologies and Virtual Mobile Networks (ICICV) (pp. 119-126). IEEE.
15. Kaur, C., Kumar, M. S., Anjum, A., Binda, M. B., Mallu, M. R., & Al Ansari, M. S. (2023). Chronic kidney disease prediction using machine learning. Journal of Advances in Information Technology, 14(2), 384-391.
16. Lohiya, A., Aggarwal, V., Dixit, A., Srivastav, R., Yadav, S., & Aarif, M. (2023). An Exploring the Relationship Between Consumer Knowledge and Adoption of Energy-Efficient Home Technologies. Journal of Informatics Education and Research, 3(2).
17. P. Soundarraj, M. Aarif, S. Gangadharan, S. R. Naqvi, N. K. AssiHalaf and A. Salih Mahdi, "Smart Product Packing and IoT Marketing: Enhancing Customer Interaction," 2023 International Conference on Innovative Computing, Intelligent Communication and Smart Electrical Systems (ICSES), Chennai, India, 2023, pp. 1-6, doi: 10.1109/ICSES60034.2023.10465408.
18. Khan, S. I., Kaur, C., Al Ansari, M. S., Muda, I., Borda, R. F. C., & Bala, B. K. (2023). Implementation of cloud based IoT technology in manufacturing industry for smart control of manufacturing process. International Journal on Interactive Design and Manufacturing (IJIDeM), 1-13.
19. Ambashtha, K. L., Vijayalakshmi, N. S., Aarif, M., Jeevalatha, R., Kuchipudi, R., & Reddy, T. S. K. (2023, December). Integrating a Neural Network Model based on LSTM and Auto Encoder into the Travel and Tourism Industry. In 2023 2nd International Conference on Automation, Computing and Renewable Systems (ICACRS) (pp. 623-628). IEEE.

20. Abd Algani, Y. M., Caro, O. J. M., Bravo, L. M. R., Kaur, C., Al Ansari, M. S., & Bala, B. K. (2023). Leaf disease identification and classification using optimized deep learning. Measurement: Sensors, 25, 100643.
21. Jiang, F., Shen, Y., Qi, G., Jing, W., Li, X., Yare, S. and Li, X., 2021. Hydrodynamics characteristics and particle distribution in a liquid–solid circulating fluidized bed boiler. Powder Technology, 377, pp.41-54.
22. Peng, J., Sun, W., Han, H. and Xie, L., 2021. CFD modeling and simulation of the hydrodynamics characteristics of coarse coal particles in a 3D liquid-solid fluidized bed. Minerals, 11(6), p.569.
23. Nelson, M., Srabet, S., Nan, T., Pjontek, D. and Zhu, J., 2022. Modified correlation for minimum fluidization velocity of low-density particles in inverse liquid–solid fluidized beds.Particuology, 71, pp.56-62.
24. Ramirez-Munoz, J., Guadarrama-Perez, R., Alvarado-Lassman, A., Valencia-Lopez, J.J. and Márquez-Baños, V.E., 2021. CFD study of the hydrodynamics and biofilm growth effect of an anaerobic inverse fluidized bed reactor operating in the laminar regime. Journal of environmental chemical engineering, 9(1), p.104674.
25. Wang, L., 2020. Extended study of the inverse fluidized bed bioreactor for low C/N ratio wastewater treatment and hydrodynamics.
26. Zhu, L., Song, Y., Chen, H., Hu, X., Zhao, C., Ai, T., Liu, Z. and Wei, X., 2023. Hydrodynamic characteristics of central pulse gas-liquid-solid circulating fluidized bed: Effect of gas and solid parameters. Powder Technology, 429, p.118922.
27. Shabandokht, M., Binaeian, E. and Tayebi, H.-A., 2016. Adsorption of food dye Acid red 18 onto polyaniline-modified rice husk composite: isotherm and kinetic analysis. Desalination and Water Treatment, 57, pp. 27638-27650.
28. Kenes, K. Y., and Yerlan, D., 2012. Study on the effectiveness of thermally treated rice husks for petroleum adsorption. Journal of Non-Crystalline Solids, 358(22), pp. 2964-2969.
29. Malafatti, J. O., Neves, T. R., and Mascarenhas, B. C., 2023. Modified Silica Nanoparticles from Rice Husk Supported on Polylactic Acid as Adsorptive Membranes for Dye Removal. Materials, 16(6), pp. 2429.
30. Tawfik, M. H. M., Refaat Diab. M., and Mohmed Abdelmotalib, H., 2019. An experimental investigation of wall-bed heat transfer and flow characteristics in a swirling fluidized bed reactor. Applied Thermal Engineering, 155, pp. 501–507.
31. Yahya, M. D., Aliyu, A. S., and Obayomi, K. S., Olugbenga, G., and Abdullah, U. B 2020. Column adsorption study for the removal of chromium and manganese ions from electroplating wastewater using cashew nutshell adsorbent. Chemical Engineering, 7(1).
32. Bayuo, J., Pelig-Ba, K. B., and Abukari, M. A., 2019. Adsorptive removal of chromium(VI) from aqueous solution unto groundnut shell. Applied Water Science, 9, 107.
33. Ouyang, D., Zhuo, Y., Hu, L., Zhang, Q., Hu, Y., and He, Z., 2019. Research on the Adsorption Behavior of Heavy Metal Ions by Porous Material Prepared with Silicate Tailings. Minerals, 9(5), 291.
34. Bhuyan, S.C., Swain, A.K., Sahoo, A. and Bhuyan, S.K., 2020. Nutrient (sulphate) removal from wastewater in inverse fluidized bed biofilm reactor. Materials Today: Proceedings, 33, pp.5476-5480.
35. Kwong, K.Y. and Marek, E.J., 2021. Combustion of biomass in fluidized beds: a review of key phenomena and future perspectives. Energy & Fuels, 35(20), pp.16303-16334.
36. Cai, Q. Q., Lee, B. C. Y., Ong, S. L., and Hu, J. Y., 2021. Fluidized-bed Fenton technologies for recalcitrant industrial wastewater treatment–Recent advances, challenges and perspective. Water Research, 190, p.116692.
37. Díaz-Heras, M., Barreneche, C., Belmonte, J.F., Calderón, A., Fernández, A.I. and Almendros-Ibáñez, J.A., 2020. Experimental study of different materials in fluidized beds with a beam-down solar reflector for CSP applications. Solar Energy, 211, pp.683-699.
38. Li, L., Duan, L., Yang, Z. and Zhao, C., 2020. Pressurized oxy-fuel combustion characteristics of single coal particle in a visualized fluidized bed combustor. Combustion and Flame, 211, pp.218-228.